Environmental Pollution 390 (2026) 127483

Contents lists available at ScienceDirect

Environmental Pollution

journal homepage: www.elsevier.com/locate/envpol

Understanding the mechanisms of coastal $PM_{2.5}$ formation driven by land-sea breeze recirculation and ship emissions☆

Jung-Woo Yoo [a], Soon-Young Park [b], Jiseon Kim [c], Daeun Chae [c], Jeonghyeok Moon [d], Cheol-Hee Kim [a,e], Jeongho Park [f], Tae-Hyeung Kim [g], Soon-Hwan Lee [a,h,*]

[a] Institute of Environmental Studies, Pusan National University, Busan, 46241, Republic of Korea
[b] Department of Science Education, Daegu National University of Education, Daegu, 42411, Republic of Korea
[c] Department of Earth Science, Pusan National University, Busan, 46241, Republic of Korea
[d] Environmental Planning Institute, Seoul National University, Seoul, 08826, Republic of Korea
[e] Department of Atmospheric Sciences, Pusan National University, Busan, 46241, Republic of Korea
[f] Department of Environmental Engineering, Gyeongsang National University, Jinju, 52725, Republic of Korea
[g] Gyeongnam Provincial Government Institute of Health and Environment, Jinju, 52732, Republic of Korea
[h] Department of Earth Science Education, Pusan National University, Busan, 46241, Republic of Korea

ARTICLE INFO

Keywords:
Sea breeze
Recirculation
Ship emissions
Source contribution
$PM_{2.5}$

ABSTRACT

Coastal cities experience persistent air pollution episodes driven by mesoscale circulation such as land-sea breezes, which can recirculate pollutants and intensify near-surface concentrations. This study quantitatively evaluated the impact of pollutant recirculation influenced by land-sea breeze circulation and ship emissions on high $PM_{2.5}$ episodes in Busan, South Korea. The Recirculation Index (RI) from 2016 to 2024 was analyzed, and April had the highest values, indicating a high potential for recirculation-related air pollution. April 2019 was selected, when recirculation events coincided with high $PM_{2.5}$ concentrations. Weather Research and Forecasting (WRF) and Community Multiscale Air Quality (CMAQ) simulations for two high pollution cases (April 7 and 21) revealed that $PM_{2.5}$ was recirculated between land and sea by diurnal land-sea breeze circulation, sustaining high concentrations in both cases. However, differences in boundary layer development, sea breeze direction, and vertical mixing intensity influenced by synoptic conditions and Busan's coastal geography with southern and eastern coastlines altered the transport pathways and spatial patterns of elevated $PM_{2.5}$. Integrated Process Rate (IPR) analysis showed that a deeper boundary layer (April 7) enhanced vertical mixing, whereas a shallower boundary layer (April 21) trapped pollutants near the surface, prolonging high concentrations. Source apportionment indicated that ship emissions contributed 0.2–14 % to $PM_{2.5}$, and recirculation enhanced $PM_{2.5}$ and sulfate concentrations by 1.4 and 3.6 %, respectively. The RI is practical for evaluating the recirculation potential. These findings highlight the role of land-sea breeze recirculation in amplifying ship emissions and underscore the need for targeted coastal emission-control strategies.

1. Introduction

Emissions and meteorological factors influence the occurrence of episodes of high air pollution (Jacob and Winner, 2009; Chen et al., 2018; Chang et al., 2021). Stagnant or weak-wind conditions frequently constrain horizontal and vertical mixing, thereby facilitating pollutant accumulation near the surface (Zhong et al., 2017; Huang et al., 2018; Lin et al., 2022; Shao et al., 2023; Han et al., 2024; Yoo et al., 2024a; Qu et al., 2024). Although the general influence of these factors has been well established, the relative importance of specific meteorological regimes remains uncertain in coastal regions, where local circulation interacts with synoptic systems.

Synoptic-scale circulation plays a critical role in regional air quality by modulating pollutant transport, atmospheric stability, and stagnation (Jeong et al., 2023; Oh et al., 2024). Weakened synoptic pressure gradients across the Korean Peninsula produce stagnant conditions that favor pollutant accumulation and secondary aerosol formation (Chang et al., 2021; Chae et al., 2025). Yoo et al. (2024b) demonstrated that cold

☆ This paper has been recommended for acceptance by Admir Créso Targino.

* Corresponding author. Department of Earth Science Education, Pusan National University, Busan, 46241, Republic of Korea.
E-mail address: withshlee@pusan.ac.kr (S.-H. Lee).

https://doi.org/10.1016/j.envpol.2025.127483
Received 28 August 2025; Received in revised form 30 November 2025; Accepted 1 December 2025
Available online 2 December 2025
0269-7491/

front passages and synoptic patterns significantly influenced pollutant transport over the Korean Peninsula. Under non-stagnant conditions, pollutant episodes can result from regional or long-range transport (Yu et al., 2020), and Yoo et al. (2022) showed that low-pressure systems associated with lee troughs enhance long-range pollutant inflow. More recently, quasi-biweekly variations in large-scale atmospheric circulation have been identified as another important driver of $PM_{2.5}$ variability in East Asia (Lee et al., 2025).

Mesoscale circulation strongly influences coastal air quality by controlling of pollutant transport and sea breeze-induced recirculation. Choi et al. (2024) linked mesoscale wind regimes to high $PM_{2.5}$ episodes over the Korean Peninsula. Yoo and Lee (2025) demonstrated that recirculation driven by land-sea breeze circulation intensified ozone pollution during stagnant summer periods in the Korean Peninsula. Land-sea breeze occurrences have been increasing across East Asia due to stronger land-sea thermal contrasts and weaker background winds (Meng et al., 2024; Huang et al., 2025). However, the combined effects of recirculation and local emission sources on coastal $PM_{2.5}$ pollution remain poorly understood.

Pollutant recirculation driven by the land-sea breeze circulation can substantially enhance coastal pollution. Pollutants transported offshore by nocturnal land breezes may return inland with the onset of daytime sea breezes, as observed in coastal regions, such as Busan, Houston, and Tianjin, which intensify pollutant accumulation under stagnant meteorological conditions (Lee et al., 2015; Chao et al., 2025; Yoo and Lee, 2025). Chao et al. (2025) reported that $PM_{2.5}$ concentrations in Houston, U.S., were approximately 30 % higher on days with recirculation linked to land-sea breezes. During such periods, ship emissions over adjacent seas can be advected inland by sea breezes, further deteriorating coastal air quality. In East Asian coastal regions, ship emissions increase $PM_{2.5}$ concentrations by up to 5 μg m^{-3} and account for 1–13 % of total $PM_{2.5}$, depending on season and location (Chen et al., 2017; Lv et al., 2018). In Busan, South Korea, ship emissions significantly contribute to air quality deterioration in port areas (Kwon et al., 2023), with receptor modeling confirming their significant influence on urban aerosol composition (Jang et al., 2023). However, despite the growing recognition of these mechanisms, few studies have quantitatively evaluated the combined effects of recirculation and ship emissions on $PM_{2.5}$ pollution in coastal regions using integrated modeling approaches.

Therefore, using a numerical modeling approach, this study quantitatively investigates how land-sea breeze–driven recirculation and ship emissions interact to influence coastal $PM_{2.5}$ pollution over South Korea. Although the effects of each factor have been examined individually, their combined impact on the complex coastal meteorological conditions remains insufficiently understood. A quantitative understanding of these coupled processes is essential for elucidating the mechanisms governing coastal air pollution and for supporting the development of region–specific mitigation strategies.

2. Methods

2.1. Meteorological and air quality observational data

This study assessed the potential pollutant recirculation in Busan by integrating meteorological and air quality measurements. The hourly wind speed and direction were obtained from the Automated Synoptic Observing System (ASOS) station in Busan (green circle in Fig. 1), which provided the basis for calculating the Recirculation Index (RI). $PM_{2.5}$ concentrations were analyzed using data from 18 Air Quality Monitoring Stations (AQMS; blue and red triangles in Fig. 1). In addition, the major components of $PM_{2.5}$, such as sulfate (SO_4^{2-}), nitrate (NO_3^-), and ammonium (NH_4^+), were collected from three intensive monitoring sites (orange stars in Fig. 1) to characterize the chemical composition of the fine particles. Observations of hourly 2-m temperature and 10-m wind speed from 17 ASOS stations (green and black circles in Fig. 1) were employed to evaluate the performance of the meteorological model. To evaluate the air quality model performance, hourly $PM_{2.5}$ observations from 18 AQMS, along with sulfate, nitrate, and ammonium data from three intensive monitoring sites, were analyzed.

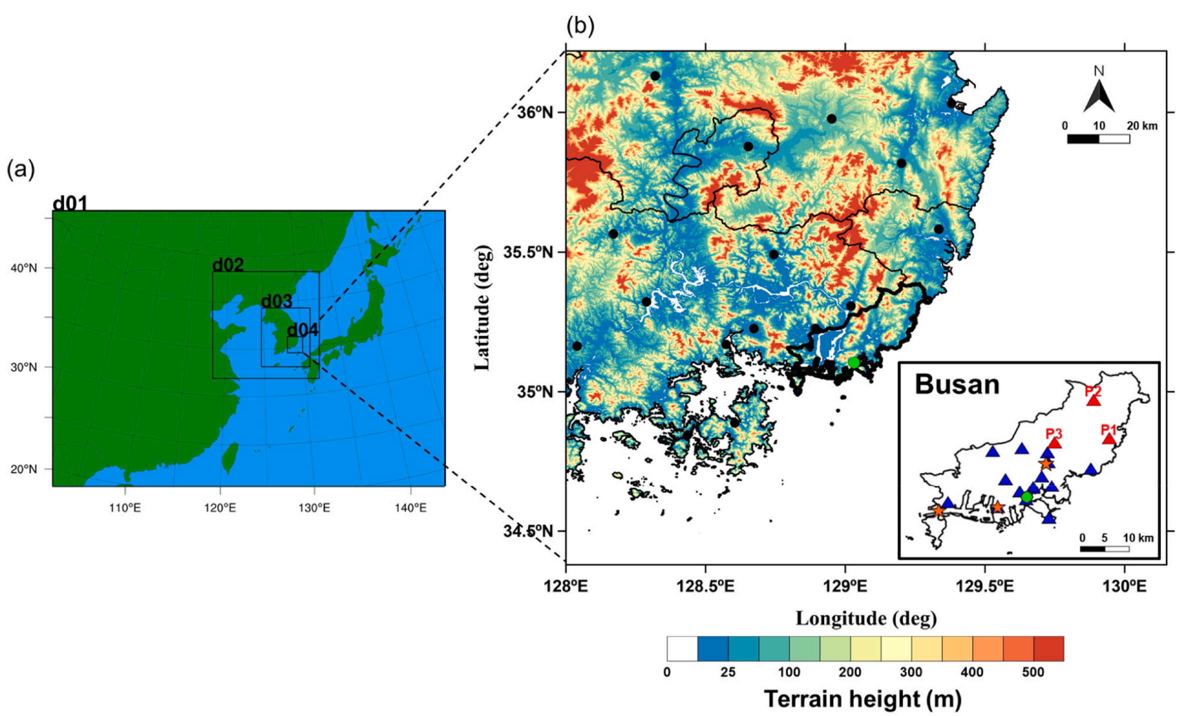

Fig. 1. (a) Modeling domains (d01-d04) used in this study. (b) Terrain height and observational sites in the innermost domain (d04). Black circles and triangles (blue and red) denote meteorological observation sites and Air Quality Monitoring Stations (AQMS), respectively. The green circle indicates the Automated Synoptic Observing System (ASOS) site in Busan, and orange stars indicate the sites measuring $PM_{2.5}$ chemical composition. (For interpretation of the references to color in this figure legend, the reader is referred to the Web version of this article.)

2.2. Meteorological and air quality model

The Weather Research and Forecasting (WRF; Skamarock et al., 2008) and Community Multiscale Air Quality (CMAQ; Byun and Schere, 2006) models were applied to investigate the influence of land-sea breeze circulation on air quality. The initial and boundary conditions for the WRF model were obtained from the NCEP FNL dataset (0.25° × 0.25°, 6-h intervals). To resolve mesoscale circulations, particularly sea breeze development, the innermost domain (d04) was configured with a 1-km horizontal resolution (Fig. 1). The Yonsei University planetary boundary layer (PBL) scheme (Hong et al., 2006), which has shown good performance in simulating coastal land-sea breeze circulations (He et al., 2022; Yoo and Lee, 2025), was applied. The Morrison double-moment microphysics (Morrison et al., 2009) and RRTMG radiation (Iacono et al., 2008) schemes were adopted. The detailed WRF model configurations are summarized in Table S1. Terrain and land-use data were derived from the default GTOPO30 and MODIS 30 s datasets. Model simulations were performed for March 21 to May 2, 2019, which included the period with the highest recirculation potential (April 2019) identified in Section 3.1. The initial 10 days (March 21–31) were used as the spin-up period to minimize the influence of the initial conditions.

The Global Air Pollutant Emissions dataset from the Emissions Database for Global Atmospheric Research (EDGAR v6.1; Crippa et al., 2022) was used for the foreign anthropogenic emissions. The Clean Air Policy Support System (CAPSS; National Institute of Environmental Research, Republic of Korea) 2019 inventory was used for domestic emissions, and the Model of Emissions of Gases and Aerosols from Nature (MEGAN v2.1) was used for biogenic emissions. The default initial chemical and boundary condition profiles of CMAQ were applied. Carbon Bond 05 with toluene chemistry (CB05-TUCL; Sarwar et al., 2008; Whitten et al., 2010) was used for the gas-phase chemistry, and the AERO6 module (Appel et al., 2013) was employed to represent the aerosol processes.

In this study, the Process Analysis module of CMAQ was applied to quantify the relative influence of physical and chemical processes on variations in $PM_{2.5}$ (Gipson and Young, 1999). To analyze the mechanisms of pollutant recirculation under land-sea breeze conditions, we applied the Integrated Process Rate (IPR) method, which enables a detailed attribution of changes in $PM_{2.5}$ to individual physical and chemical processes. The assessment accounted for transport and mixing pathways, including horizontal advection (HADV), vertical advection (ZADV), horizontal diffusion (HDIF), vertical diffusion (VDIF), and emissions (EMIS). This approach enabled the identification of the dominant processes responsible for the changes in $PM_{2.5}$ concentrations. IPR calculations were performed for grid cells covering Busan, and the results were averaged to represent regional-scale characteristics.

2.3. Calculation of the Recirculation Index

To quantitatively assess the potential for pollutant recirculation associated with land-sea breeze circulation, the RI was calculated according to Allwine and Whiteman (1994). The RI expresses the ratio of the total travel distance to the net displacement of air parcels using hourly wind observations at a single location, and is defined as

$$L = \sqrt{\left(\sum_{j=i}^{i-\tau+1} T \times u_j\right)^2 + \left(\sum_{j=i}^{i-\tau+1} T \times v_j\right)^2} \tag{1}$$

$$S = \sum_{j=i}^{i-\tau+1} \sqrt{(T \times u_j)^2 + (T \times v_j)^2} \tag{2}$$

$$RI = 1 - \frac{L}{S} \tag{3}$$

where T is the total time period (24 h); u_j and v_j represent the zonal and meridional wind components at each hour, respectively; L is the net displacement; and S is the total distance traveled. RI values approaching zero indicate predominantly linear transport, whereas values approaching one reflect a high potential for recirculation. Although this method does not explicitly account for vertical mixing, it provides a widely used quantitative metric for characterizing the horizontal recirculation under land-sea breeze conditions (Wang et al., 2022). This approach has been extensively applied in coastal air quality studies in the U.S. (Li et al., 2020), Portugal (Russo et al., 2016), China (Li et al., 2018; Wang et al., 2022; Huang et al., 2025), and the Korean Peninsula (Lee et al., 2015; Yoo and Lee, 2025) to investigate the relationship between recirculation events and air pollution.

In this study, the RI values were calculated using wind data from the Busan ASOS station for 2016–2024. Months with frequent recirculation events were identified based on the RI, and representative high-RI cases were selected for detailed numerical simulations.

2.4. Experimental design

In this study, numerical simulations using the WRF and CMAQ models were conducted from March 21 to May 1, 2019. The period from March 21 to March 31 was designated as the spin-up period, and the analysis focused on the simulation results for April 2019.

According to the 2019 CAPSS emissions inventory, the annual emissions from the Busan region were estimated to be 47,811 tons of NOx, 9,098 tons of SOx, 5,888 tons of PM_{10}, and 2,469 tons of $PM_{2.5}$. Of these, ship emissions accounted for approximately 40 %, 75 %, 21 %, and 46 % of NOx, SOx, PM_{10}, and $PM_{2.5}$, respectively (Fig. S1), indicating a potentially significant contribution of ship emissions to the air pollution in Busan.

Three numerical experiments were conducted to quantitatively assess the impact of ship emissions under conditions of high recirculation potential:

(1) Base experiment: Simulation including all emissions from domestic (including Busan), foreign, and ship sources
(2) BusanShip experiment: Simulation including emissions from Busan and ships, excluding foreign sources
(3) BusanOnly experiment: Simulation including emissions from Busan only, excluding foreign and ship sources

The source contributions were calculated using the concentration differences among the three experiments, as defined below:

$$Contribution_{external}(\%) = \frac{C_{Base} - C_{BusanShip}}{C_{Base}} \times 100 \tag{4}$$

$$Contribution_{ship}(\%) = \frac{C_{BusanShip} - C_{BusanOnly}}{C_{Base}} \times 100 \tag{5}$$

$$Contribution_{busan}(\%) = \frac{C_{BusanOnly}}{C_{Base}} \times 100 \tag{6}$$

where C represents the simulated $PM_{2.5}$ concentrations in each experiment.

3. Results

3.1. Monthly variation of RI and $PM_{2.5}$ (2016–2024)

Fig. 2a shows the monthly variations in the RI and $PM_{2.5}$ concentrations in Busan from 2016 to 2024. The RI was the highest in April (0.29) and lowest in July (0.19). $PM_{2.5}$ concentrations peaked in January and March (24.67 μg m^{-3}) and were lowest in September (13.22 μg m^{-3}). April exhibited the highest average RI among all months, suggesting favorable conditions for pollutant recirculation associated with land-sea breeze circulation. Sea breeze events occur

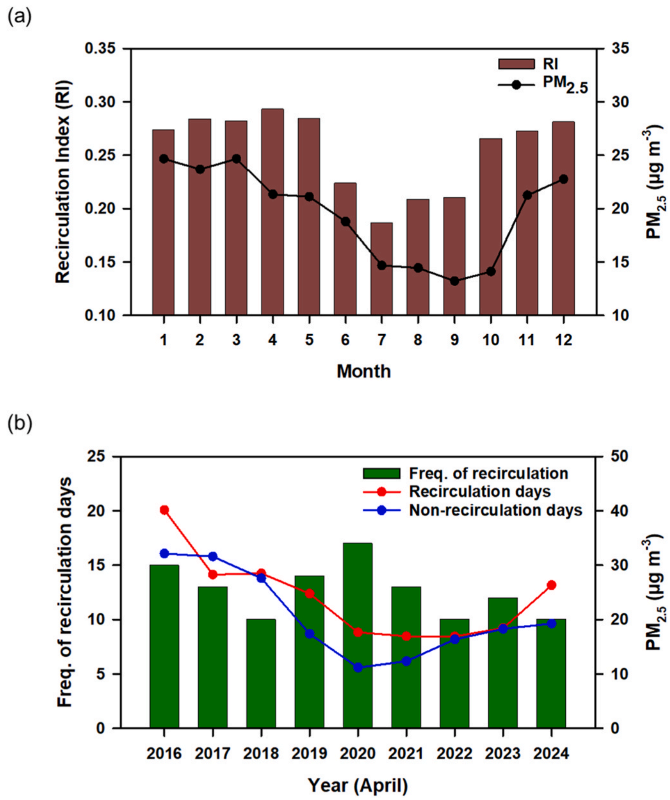

Fig. 2. (a) Monthly mean Recirculation Index (RI) and $PM_{2.5}$ concentrations from 2016 to 2024. (b) Frequency of recirculation days and mean $PM_{2.5}$ concentrations on recirculation and non-recirculation days in April during 2016–2024.

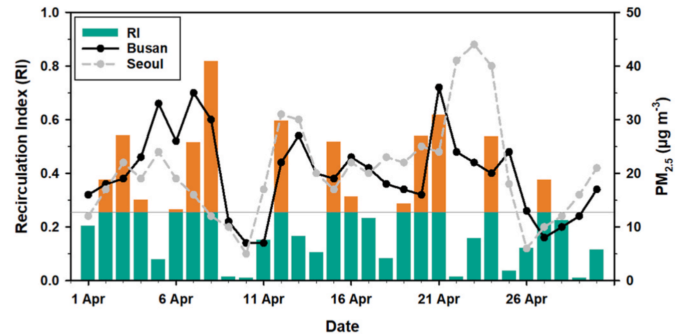

Fig. 3. Daily Recirculation Index (RI) and mean $PM_{2.5}$ concentrations in Busan and Seoul during April 2019.

most frequently from spring to early summer, when land surfaces warm more rapidly than the sea owing to increased solar radiation (Viner et al., 2021). These seasonal characteristics indicate that April provides an optimal period for examining recirculation mechanisms and the associated $PM_{2.5}$ variability.

Following Russo et al. (2018) and Yoo and Lee (2025), the recirculation days were defined as the days when the daily RI exceeded the long-term mean RI calculated for the study period. In this study, recirculation days were defined as days with an RI equal to or greater than the long-term average (0.254) calculated from 3,288 days between 2016 and 2024.

Fig. 2b illustrates the annual variation in the number of recirculation days and the mean $PM_{2.5}$ concentrations on recirculation and non-recirculation days in April for 2016–2024. Although the number of recirculation days fluctuated annually, >10 such days were consistently identified each April, with particularly high frequencies in 2016, 2019, and 2020. In most years, $PM_{2.5}$ concentrations were higher on recirculation days than on non-recirculation days, with the largest differences observed in April 2016 (8.0 μg m^{-3}) and April 2019 (7.4 μg m^{-3}). These findings suggest that recirculation processes contributed significantly to particulate matter accumulation during these periods.

April 2016 included five days affected by Asian dust, which likely increased the $PM_{2.5}$ concentrations during this period. In contrast, no Asian dust events occurred in April 2019, allowing the differences between recirculation and non-recirculation days to be distinguished more clearly. Therefore, April 2019 was selected as the case study period for detailed simulations aimed at investigating land-sea breeze associated recirculation and its contribution to $PM_{2.5}$ pollution in Busan.

Fig. 3 shows the daily variation in the RI and $PM_{2.5}$ concentrations in Busan and Seoul during April 2019. Seoul was included in the analysis because it is strongly influenced by transboundary pollution (Choi et al., 2024), thereby providing a reference point for distinguishing transboundary sources from local emissions in Busan. By comparing the two cities, the influence of land-sea breeze circulations and associated pollutant transport on high $PM_{2.5}$ episodes in Busan can be elucidated. In Fig. 3, daily RI values are represented as vertical bars, with green and orange bars indicating days below and above (recirculation days) the mean threshold of 0.254, respectively. April 2019 had 14 recirculation days. A correlation coefficient (R) of approximately 0.41 was identified between $PM_{2.5}$ concentrations and the RI in Busan, suggesting that higher RI values are associated with higher $PM_{2.5}$ concentrations. This relationship indicates that enhanced recirculation may promote the transport and accumulation of pollutants, leading to higher $PM_{2.5}$ concentrations under certain meteorological conditions. However, this correlation should be interpreted cautiously, given the limited temporal scope of the one-month analysis.

On April 7 and 21, RI values exceeded 0.5 and daily mean $PM_{2.5}$ concentrations in Busan surpassed 35 μg m^{-3}. Meanwhile, $PM_{2.5}$ concentrations in Seoul were substantially lower (16 and 24 μg m^{-3}, respectively), confirming that the high pollution in Busan was primarily driven by local circulations rather than transboundary transport. Therefore, these days were selected for detailed analysis, as they clearly demonstrated the influence of mesoscale circulations, specifically land-sea breeze recirculation, on $PM_{2.5}$ buildup under weak synoptic forcing.

3.2. *Model performance evaluation*

Before the detailed modeling analysis of the April 2019 case, we evaluated the performance of the WRF and CMAQ simulations to ensure that the meteorological and air quality conditions were realistically reproduced. The statistical metrics used in this study included the mean bias (MB), which represents the average difference between the modeled and observed values; root mean square error (RMSE), which measures the magnitude of the overall error; index of agreement (IOA), which quantifies the level of agreement on a scale from 0 to 1, and R, which indicates the linear correlation, with values closer to 1 denoting stronger correlation.

The meteorological simulations satisfied the performance criteria suggested by Emery et al. (2001), which require MB $\leq\pm$ 0.5 °C and IOA $\geq$0.7 for 2-m temperature, and MB $\leq\pm$ 0.5 m s^{-1} and IOA $\geq$0.6 for 10-m wind speed. The simulated 2-m temperature showed excellent agreement with an IOA of 0.95 and R of 0.92, whereas the 10-m wind speed simulation showed satisfactory accuracy with an IOA of 0.73 and R of 0.65 (Fig. S2). Additionally, the RMSEs were 2.05 °C for 2-m temperature and 1.68 m s^{-1} for 10-m wind speed, further supporting the reliability of the WRF simulations.

The $PM_{2.5}$ concentrations simulated using the CMAQ model was compared with surface observations (Fig. S3). The observed and modeled mean $PM_{2.5}$ concentrations in April 2019 were 18.79 and 18.43 μg m^{-3}, respectively. The statistical indicators showed RMSE = 13.18 μg m^{-3}, MB = −0.37 μg m^{-3}, IOA = 0.72, and R = 0.60, indicating that the model reasonably reproduced temporal variations with a slight underestimation. The major ionic components (sulfate, nitrate, and ammonium) were also slightly underestimated but exhibited IOA and R values exceeding 0.6, indicating an overall reliable model performance. This bias likely resulted from uncertainties in emissions, meteorological inputs, and boundary conditions (Miao et al., 2017). In particular, the overestimated wind speeds in the WRF model (Fig. S2) may have enhanced the horizontal dispersion, leading to lower near-surface $PM_{2.5}$ concentrations. Overall, the model reproduced the observed variations reasonably well, providing confidence in subsequent source contribution and process analyses.

3.3. Analysis of high $PM_{2.5}$ episodes under land-sea breeze influence

The synoptic surface weather patterns for April 7 and 21 are shown in Fig. S4. On both days, a high-pressure system dominated the Korean Peninsula, providing favorable conditions for mesoscale circulation such as land-sea breezes. However, differences in the pressure distribution and relative positions of the surrounding high- and low-pressure systems around the Korean Peninsula likely influenced the direction and strength of local sea breeze development and the associated pollutant transport.

On April 7, a high-pressure system extending from northern China and a weak low-pressure system extending to the southwest formed a weak east-west pressure gradient over the Busan area, favoring the development of an easterly sea breeze. This sea breeze circulation could have transported pollutants from the sea back toward land, contributing to locally elevated $PM_{2.5}$ concentrations.

In contrast, April 21 was characterized by a broad high-pressure system covering the Korean Peninsula, with Busan located near the southeastern edge of the system, where widely spaced isobars indicated weak synoptic forcing. Although a weak low-pressure system was present to the east of the peninsula, the pressure difference between the two systems was small, resulting in a weak pressure gradient over Busan. This synoptic pattern provided favorable conditions for the development

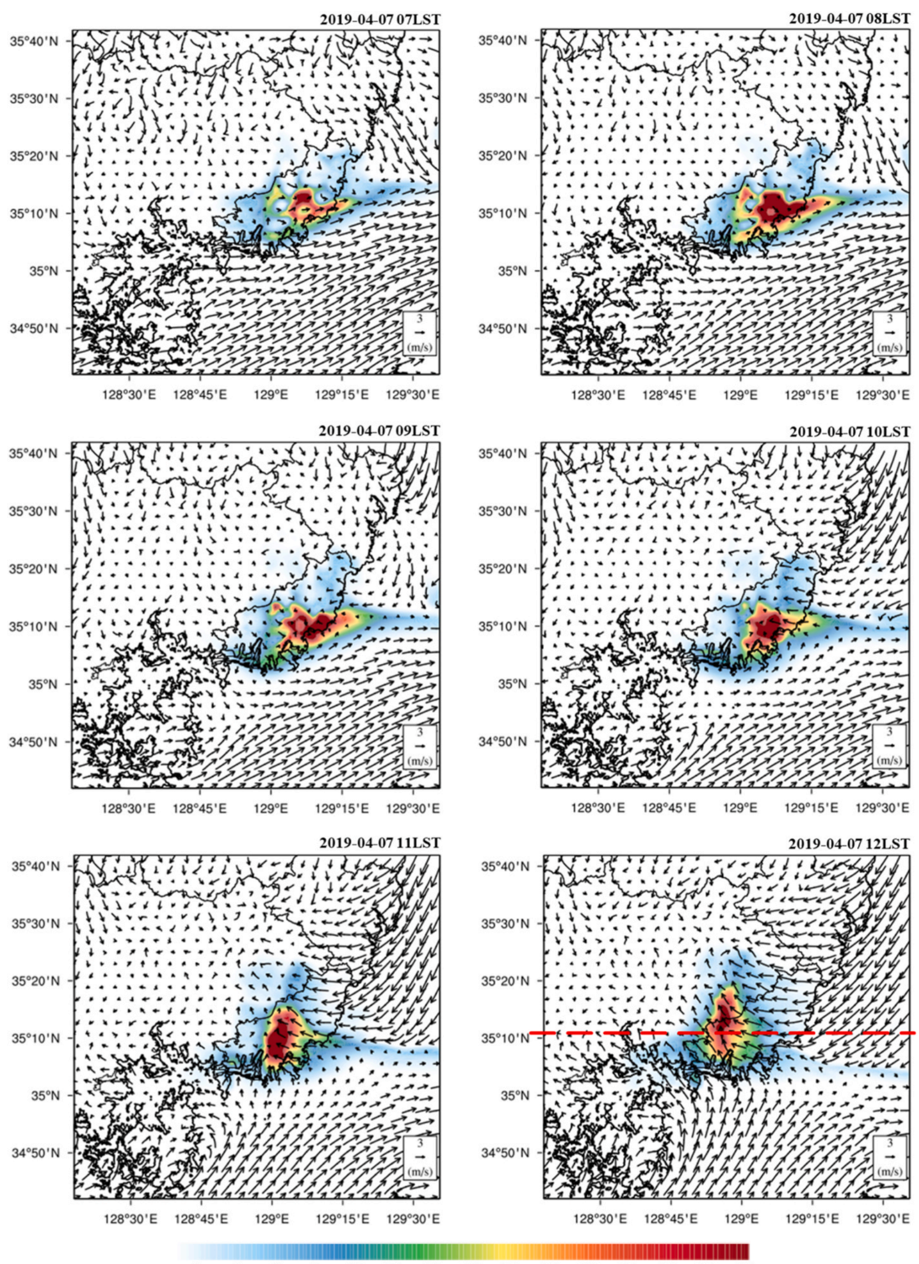

Fig. 4. Horizontal distribution of $PM_{2.5}$ concentrations from the BusanOnly experiment on April 7, 2019.

of local circulation, such as land-sea breezes. The weak cyclonic flow associated with the low-pressure system in the east may have enhanced the southerly component of the sea breeze. Under this weak synoptic forcing, a southerly sea breeze developed over the Busan area, which is consistent with previous observations that southerly sea breezes were dominant along the southeastern Korean coast (Oh et al., 2006; Park et al., 2014). However, southerly and easterly sea breeze components can develop under weak synoptic conditions, depending on the local topography and coastal orientation. Therefore, the contrasting sea breeze directions observed on April 7 and 21 reflect the representative behavior of local land-sea breeze circulation under different synoptic patterns and coastal topographies.

3.3.1. Case 1: April 7

To investigate the recirculation of pollutants emitted by Busan back into the city, we analyzed the horizontal distribution of $PM_{2.5}$ concentrations from 07:00 to 12:00 on April 7, 2019, using the BusanOnly experiment, which included emissions only from the Busan area (Fig. 4). During 07:00–08:00, weak westerly (offshore) winds slowly transported pollutants from land toward the sea, leading to elevated $PM_{2.5}$ concentrations along the coast and in nearby offshore regions of Busan. Sea breeze circulation began to develop around 09:00, and after 10:00, an easterly sea breeze became more prominent, recirculating $PM_{2.5}$ from the sea back to land.

To quantify sea breeze development and the associated $PM_{2.5}$ changes, the time series of wind speed, direction, and $PM_{2.5}$ concentrations over Busan from the Base experiment were analyzed (Fig. 5a). Horizontal distribution analysis showed that sea breezes began to develop at approximately 09:00. Accordingly, the $PM_{2.5}$ peak observed at 08:00 is likely attributable to the combined influence of pollutants accumulated during the night and early morning hours and local emissions within Busan (Fig. 5a). In contrast, the 11:00 peak, which occurred after the development of the sea breeze, can be attributed to the recirculation of pollutants that had been transported to the sea by the nocturnal land breeze, and subsequently recirculated inland by the sea breeze. This pattern indicates that high concentrations were generated through the return of pollutants previously transported to the sea, driven by land-sea breeze recirculation.

The east-west vertical cross-section along 35.18° N (Fig. 4) also reveals consistent characteristics of land-sea breeze circulation (Fig. 6). During 07:00–08:00, weak westerlies transported $PM_{2.5}$ offshore; however, the wind direction near the coastline gradually shifted inland over time. After 10:00, fully developed easterly sea breezes transported of $PM_{2.5}$ from the sea. At 11:00 LST, a sea breeze front formed at the location where the potential temperature (Fig. 6) over the sea (308 K) intersected with that over land (308 K), and elevated $PM_{2.5}$ concentrations were observed near the front. As the sea breeze front propagated inland, the potential temperature in the lower coastal layer decreased to 306 K, indicating the advection of cooler marine air. In contrast, the inland areas maintained higher values of 308–310 K, and exhibited a distinct horizontal gradient. The PBL heights developed up to approximately 1.4 km, with a return flow toward the sea observed near the upper part of the boundary layer (1.0–1.2 km). This feature is consistent with the typical land-sea breeze structure reported in previous studies, in which onshore flow in the lower layer (surface to approximately 500 m) and upward motion above the sea breeze front led to the development of a return flow near approximately 900 hPa (Crosman and Horel, 2010; Miller et al., 2003). In this study, $PM_{2.5}$ was transported from land to sea along this return flow, whereas in the lower layer (surface to approximately 800 m), the sea breeze transported $PM_{2.5}$ inland. These processes illustrate how horizontal recirculation driven by land-sea breeze circulation, combined with boundary layer mixing, contributed

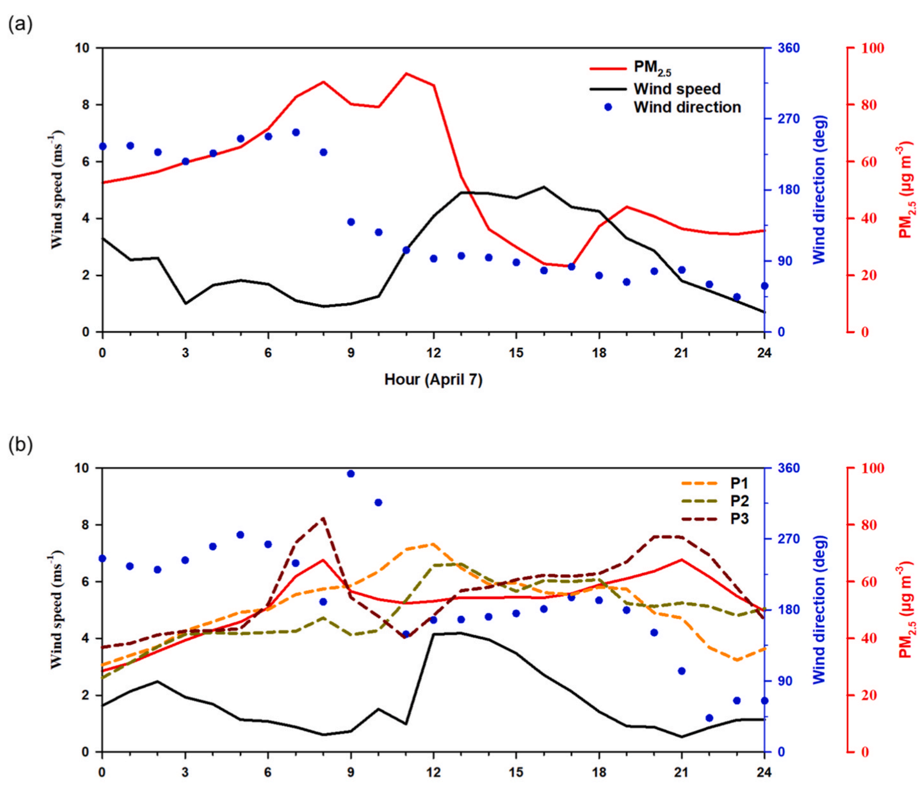

Fig. 5. Time series of wind speed, wind direction, and $PM_{2.5}$ concentrations in Busan from the Base experiment on (a) April 7 and (b) 21, 2019. Red and black solid lines indicate $PM_{2.5}$ concentrations and wind speed, respectively, whereas blue dots represent wind direction. In (b), colored dashed lines (P1–P3) denote $PM_{2.5}$ concentrations at the three eastern coastal sites shown in Fig. 1. (For interpretation of the references to color in this figure legend, the reader is referred to the Web version of this article.)

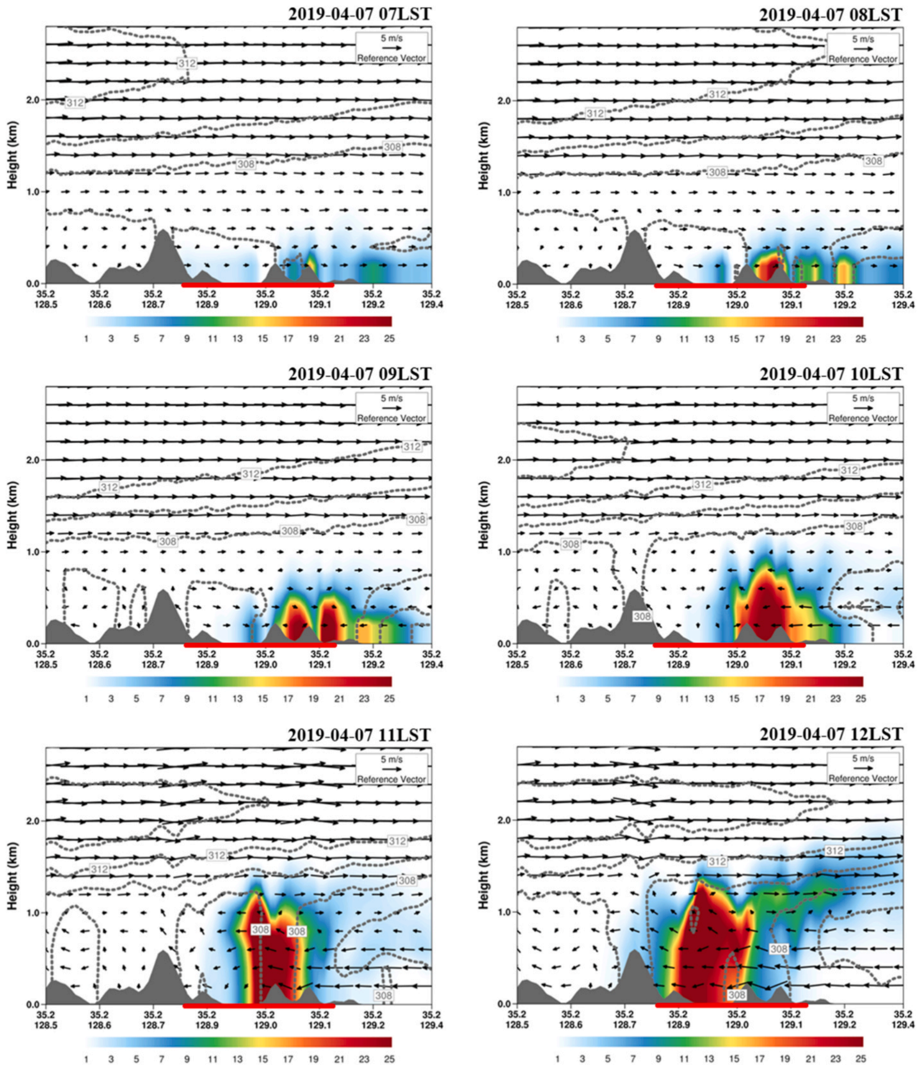

Fig. 6. Vertical cross-sections of $PM_{2.5}$ concentrations from the BusanOnly experiment on April 7, 2019. Gray dashed lines indicate potential temperature, and the red line represents Busan. (For interpretation of the references to color in this figure legend, the reader is referred to the Web version of this article.)

to elevated $PM_{2.5}$ concentrations over Busan.

According to the IPR analysis over Busan (Fig. 7a), during sea breeze intrusion (09:00–11:00 LST), positive contributions from HADV were found below approximately 400 m (layers 1–4), quantitatively confirming the inland transport of pollutants from the sea. In addition, negative contributions from ZADV appeared in layers 1–5, suggesting that the transported pollutants were mixed vertically and dispersed upward within the developing boundary layer. The formation of high $PM_{2.5}$ concentrations on April 7 can be attributed to the interaction between sea breeze-driven horizontal transport and vertical mixing within the boundary layer. This case represents an easterly sea breeze that commonly develops along the southeastern coast of Korea under

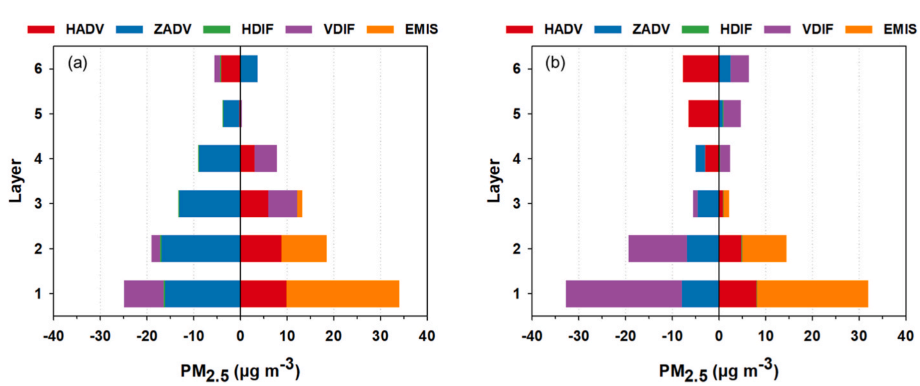

Fig. 7. Integrated Process Rate analysis showing the contributions of horizontal advection (HADV), vertical advection (ZADV), horizontal diffusion (HDIF), vertical diffusion (VDIF), and emissions (EMIS) to $PM_{2.5}$ concentrations changes during the sea breeze period (09:00–11:00 LST) on (a) April 7 and (b) 21, 2019. Height levels correspond to 28 m, 98 m, 193 m, 314 m, 466 m, and 659 m. The results represent the average of grid cells covering Busan.

weak synoptic conditions (Oh et al., 2006; Park et al., 2014).

3.3.2. Case 2: April 21

On April 21, the winds remained weak in the morning, with mean speeds of approximately 0.7 m s^{-1} in Busan. Under these conditions, pollutants were not sufficiently advected offshore by the land breeze and the atmosphere stagnated, leading to the accumulation of $PM_{2.5}$ in the coastal region (Fig. 8). After 09:00, southerly to southeasterly sea breezes gradually developed under weak synoptic forcing, which was consistent with the synoptic pattern described in Section 3.3. These locally developed breezes initiated the inland transport of accumulated $PM_{2.5}$. This transport became more apparent after 12:00, resulting in high $PM_{2.5}$ concentrations over the Busan area.

At 08:00, a peak in $PM_{2.5}$ concentrations was observed, similar to the early-morning enhancement on April 7 (Fig. 5b). However, despite the development of a southerly sea breeze at approximately 11:00, the mean $PM_{2.5}$ concentration in Busan did not increase pronouncedly. Following the development of the sea breeze, concentrations gradually increased at the eastern coastal sites (P1–P3). The increases began after 09:00 at P1, 10:00 at P2, and 11:00 at P3 (Fig. 5b). These elevated concentrations were largely confined to the eastern coastal area. This indicates that sea breezes transported pollutants inland from the eastern coastline, producing localized high concentrations. Consequently, on April 21, the southerly sea breeze primarily influenced the eastern coastal zone, resulting in localized pollution, while on April 7, the easterly sea breeze transported pollutants more broadly inland, leading to a citywide increase in mean concentrations. These findings suggest that the locations of high $PM_{2.5}$ concentrations can vary depending on the sea breeze direction and the associated transport pathways.

The north-south vertical cross section along 129.13° E confirms the inland transport of cooler air from the sea (Fig. 9). The sea breeze on April 21 extended up to an altitude of approximately 600 m, with a

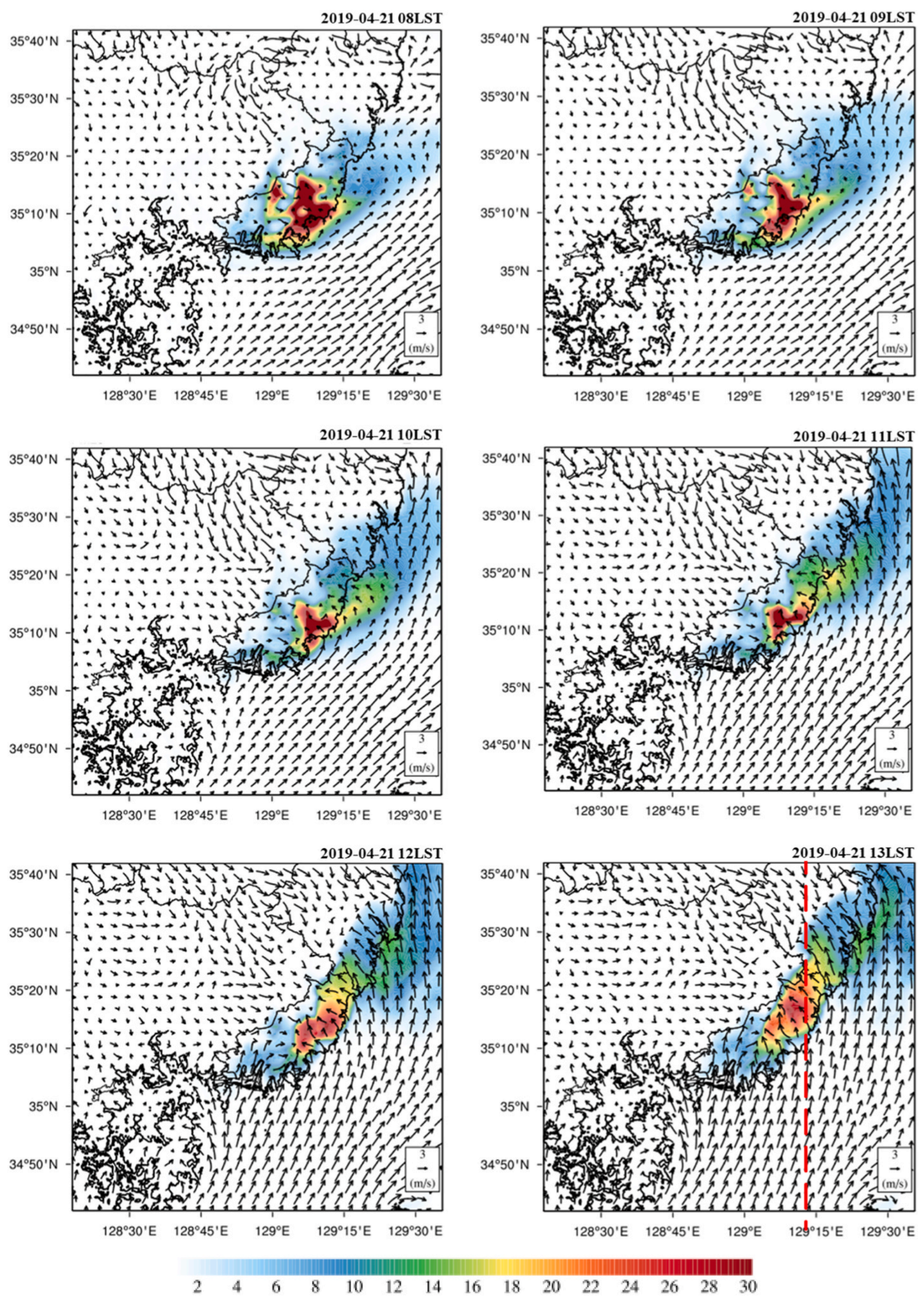

Fig. 8. Horizontal distribution of $PM_{2.5}$ concentrations from the BusanOnly experiment on April 21, 2019.

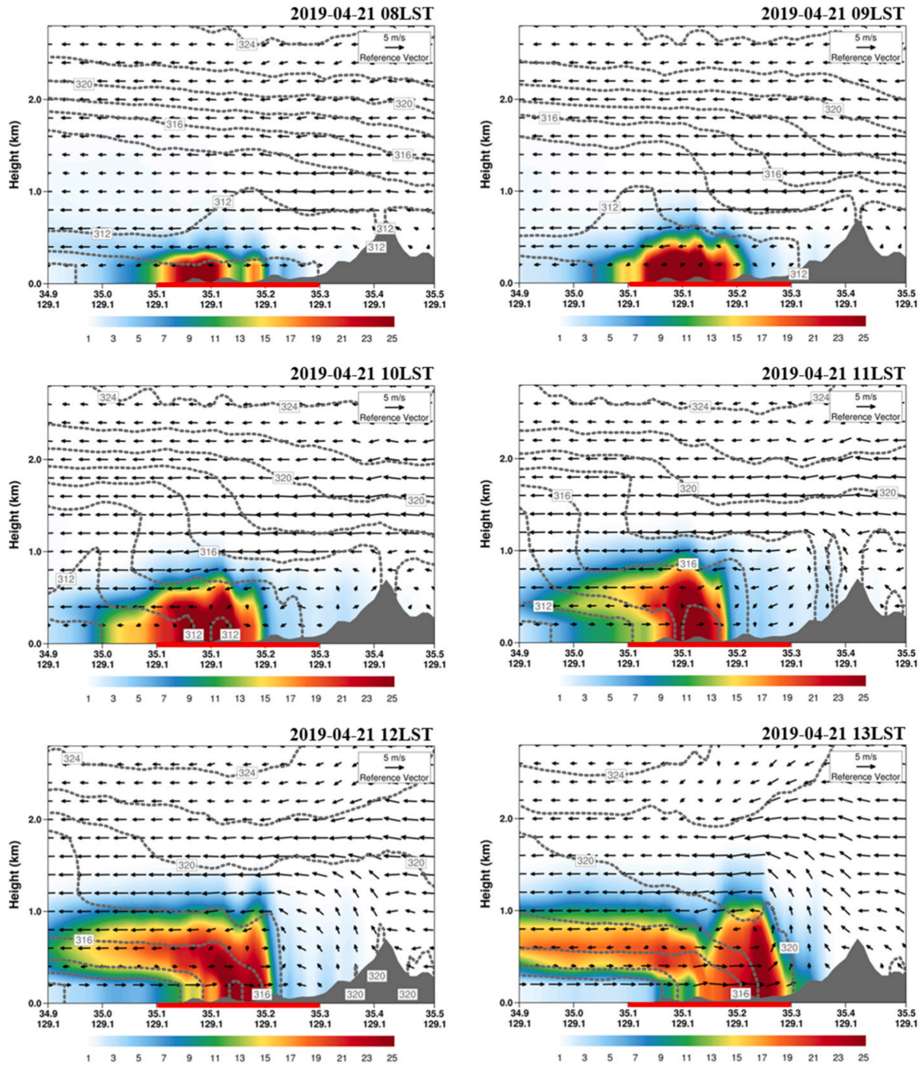

Fig. 9. Vertical cross-sections of $PM_{2.5}$ concentrations from the BusanOnly experiment on April 21, 2019. Gray dashed lines indicate potential temperature, and the red line represents Busan. (For interpretation of the references to color in this figure legend, the reader is referred to the Web version of this article.)

return flow toward the sea forming near 800 m, indicating a relatively shallow vertical structure of sea breeze circulation. On April 7, the boundary layer developed to a higher altitude and stronger vertical mixing dispersed pollutants more effectively into the upper layers, which weakened the horizontal transport toward the sea by the return flow. In contrast, on April 21, the lower boundary layer height limited vertical mixing, causing pollutants to remain concentrated in the lower layer and enabling the return flow to transport more $PM_{2.5}$ toward the sea. These differences suggest that variations in boundary layer development and vertical mixing intensity can substantially affect the amount of $PM_{2.5}$ transported from land to sea by the return flow, which in turn can influence its horizontal distribution during recirculation events.

The IPR analysis over Busan (Fig. 7b) showed that from 09:00–11:00 LST, positive HADV contributions were present, although they were limited to layers (1–2). This indicated that pollutant recirculation primarily occurred near the surface. The ZADV contributions were weakly negative in layers 1–4, suggesting shallow and limited vertical mixing, which limited the upward dispersion of pollutants. Consequently, the recirculated pollutants likely remained near the surface for longer periods, sustaining high concentrations. This is consistent with the $PM_{2.5}$ time series (Fig. 5b), which showed that, unlike those on April 7, where concentrations declined after noon, the high concentrations on April 21 persisted in the afternoon.

This case was not characterized by a typical land-to-sea breeze transition but by weak land breezes under stagnant meteorological conditions, followed by the development of a daytime sea breeze. On April 7, an easterly sea breeze developed, whereas on April 21, the sea breeze was southerly, reflecting the influence of synoptic conditions and Busan's geographic location, which is situated along the southern and eastern coastlines.

In both cases, land-sea breeze circulation contributed to $PM_{2.5}$ recirculation and high concentrations. However, variations in the boundary layer development, sea breeze intensity and direction, and vertical mixing conditions influenced the persistence and spatial distribution of elevated concentrations. Although high RI values are generally associated with recirculation events, similar values can also occur under stagnant conditions with weak winds, making it difficult to clearly identify recirculation. Therefore, incorporating additional criteria, such as wind speed, along with RI thresholds may improve the accuracy of the recirculation day classification.

3.4. Source contribution analysis

To quantify the contribution of different sources to $PM_{2.5}$ and its major components (sulfate, nitrate, and ammonium), April 2019 was categorized into recirculation and non-recirculation days. The relative contributions of external sources, ship emissions, and Busan emissions were estimated (Table S2). The contributions were estimated as relative percentages based on the differences between the model experiments.

Ship emissions accounted for an average of 3.5 % of $PM_{2.5}$, with a maximum contribution of 14.0 %. Notably, the contribution from ships was higher on the recirculation days, averaging 4.3 %, which was 1.4 % greater than that on the non-recirculation days (2.9 %). Similar trends were observed for sulfate and ammonium. During active recirculation, the pollutants that remained over the sea were likely transported inland by sea breezes, thereby enhancing the impact of ship emissions. The average contribution of ships to sulfate was 4.6 %, peaking at 42.3 %. On recirculation days, the average increased to 6.5 %, 3.6 % higher than that on non-recirculation days. Similarly, ammonium showed an average ship contribution of 3.7 % on recirculation days, which was 1.9 % higher than that on non-recirculation days. In contrast, nitrate showed lower ship contributions on the recirculation days. This may be attributed to the relatively strong influence of land-based emission sources, such as vehicle NOx, on non-recirculation days. These sources promote the formation of nitrates, thereby reducing the relative contributions of ship emissions. Additionally, under humid sea breeze conditions, weakened photochemical activity may suppress gaseous HNO_3 production, further limiting secondary nitrate formation (Ding et al., 2021; Lu et al., 2023). Overall, these results indicated that recirculation events combined with ship emissions elevated $PM_{2.5}$ concentrations in Busan, particularly sulfate and ammonium.

According to the 2019 CAPSS inventory, approximately 75 % of SOx emissions in Busan originate from ships, which is significantly higher than the proportions of NOx and $PM_{2.5}$ (Fig. S1). Therefore, when meteorological conditions, such as sea breezes, enhance the inland transport of coastal pollutants on recirculation days, the impact of ship emissions on sulfate and ammonium concentrations is amplified. These findings highlight the importance role of ship emissions in pollutant recirculation events and suggest that SOx emissions from ships, coupled with recirculation-related meteorological processes, can significantly contribute to high $PM_{2.5}$ concentrations in Busan. This emphasizes the need for emission control strategies targeting ship emissions, particularly under conditions conducive to recirculation, to improve air quality and mitigate pollution.

4. Conclusions

This study examined how land-sea breeze-driven recirculation and ship emissions interactively affect $PM_{2.5}$ pollution in Busan, South Korea, using the WRF and CMAQ models. The RI analysis indicated that April exhibited the highest potential for recirculation throughout the year. Two high $PM_{2.5}$ recirculation cases in April 2019 showed that sea breeze circulations transported pollutants inland, increasing $PM_{2.5}$. Variations in boundary layer development and sea breeze direction are influenced by synoptic forcing, coastal topography, controlled pollutant transport, and return flows within sea breeze circulation.

During recirculation events, ship emissions contributed approximately 4 % of the total $PM_{2.5}$ on average and up to 14 % at the peak, with sulfate contributions increasing from 4.6 % to 6.5 %. These results exhibit patterns consistent with those of other coastal cities, such as Qingdao (1.5–13.1 %) and Houston (30 % higher on recirculation days). However, the overall influence appeared to be weaker, likely reflecting the short study period (April) and the use of citywide averages. Nevertheless, the findings consistently suggest that meteorological conditions favorable for sea breeze recirculation amplify the influence of ship emissions and promote secondary aerosol formation in coastal areas.

These findings highlight the practical value of the RI for identifying recirculation potential and forecasting pollution episodes. Integrating the RI and short-term weather forecasts into early warning systems could support the timely control of ship emissions in port areas. However, its broader application may be constrained by limited wind data, complex topography, and variability in the boundary layer development.

Future work should refine the RI by introducing wind speed thresholds to better distinguish between recirculation and stagnation. Comparative analyses across coastal regions would help clarify its general applicability under diverse climatic and emission conditions and improve forecasting and emission-control strategies for coastal cities.

CRediT authorship contribution statement

Jung-Woo Yoo: Writing – review & editing, Writing – original draft, Methodology, Investigation, Formal analysis, Conceptualization. **Soon-Young Park:** Writing – review & editing, Formal analysis. **Jiseon Kim:** Visualization, Data curation. **Daeun Chae:** Validation, Investigation. **Jeonghyeok Moon:** Software, Methodology. **Cheol-Hee Kim:** Writing – review & editing. **Jeongho Park:** Conceptualization. **Tae-Hyeung Kim:** Conceptualization. **Soon-Hwan Lee:** Writing – review & editing, Supervision, Project administration, Funding acquisition, Conceptualization.

Declaration of competing interest

The authors declare the following financial interests/personal relationships which may be considered as potential competing interests: SOON-HWAN LEE reports financial support was provided by National Research Foundation of Korea. SOON-HWAN LEE reports financial support was provided by Korea Ministry of Science and ICT. If there are other authors, they declare that they have no known competing financial interests or personal relationships that could have appeared to influence the work reported in this paper.

Acknowledgements

This research was supported by the Basic Science Research Program through the National Research Foundation of Korea (NRF), funded by the Ministry of Education (RS-2020-NR049592) and the Korean Government (MSIT) (RS-2022-NR070051).

Appendix A. Supplementary data

Supplementary data to this article can be found online at https://doi.org/10.1016/j.envpol.2025.127483.

Glossary

Abbreviations	
ASOS	Automated Synoptic Observing System
AQMS	Air Quality Monitoring Stations
CB05TUCL	Carbon Bond 05 with Toluene Chemistry
CMAQ	Community Multiscale Air Quality model
EDGAR	Emissions Database for Global Atmospheric Research
EMIS	Emissions

(*continued on next page*)

(*continued*)

HADV	Horizontal Advection
HDIF	Horizontal Diffusion
IOA	Index of Agreement
IPR	Integrated Process Rate
MB	Mean Bias
MEGAN	Model of Emissions of Gases and Aerosols from Nature
PBL	Planetary Boundary Layer
R	Correlation Coefficient
RI	Recirculation Index
RMSE	Root Mean Square Error
VDIF	Vertical Diffusion
WRF	Weather Research and Forecasting model
ZADV	Vertical Advection

Data availability

Data will be made available on request.

References

Allwine, K.J., Whiteman, C.D., 1994. Single-station integral measures of atmospheric stagnation, recirculation and ventilation. Atmos. Environ. 28, 713–721. https://doi.org/10.1016/1352-2310(94)90048-5.

Appel, K.W., Pouliot, G.A., Simon, H., Sarwar, G., Pye, H.O.T., Napelenok, S.L., Akhtar, F., Roselle, S.J., 2013. Evaluation of dust and trace metal estimates from the community multiscale air quality (CMAQ) model version 5.0. Geosci. Model Dev. 6 (4), 883–899. https://doi.org/10.5194/gmd-6-883-2013.

Byun, D., Schere, K.L., 2006. Review of the governing equations, computational algorithms, and other components of the models-3 community multiscale air quality (CMAQ) modeling system. Appl. Mech. Rev. 59 (2), 51–76. https://doi.org/10.1115/1.2128636.

Chae, D., Yoo, J.W., Kim, J., Lee, S.H., 2025. Conceptual study on spatial distribution fluctuations of $PM_{2.5}$ concentration on the Korean Peninsula in winter related to synoptic meteorological clusters. Atmos. Environ. 356, 121288. https://doi.org/10.1016/j.atmosenv.2025.121288.

Chang, L.S., Lee, G., Im, H., Kim, D., Park, S.M., Choi, W.J., Lee, Y., Lee, D.W., Kim, D.G., Lee, D., Kim, Y.W., Kim, J., Ho, C.H., 2021. Quantifying the impact of synoptic weather systems on high $PM_{2.5}$ episodes in the Seoul metropolitan area, Korea. J. Geophys. Res. Atmos. 126 (10). https://doi.org/10.1029/2020JD034085 e2020JD034085.

Chao, C.Y., Li, W., Hopke, P.K., Guo, F., Wang, Y., Griffin, R.J., 2025. Increases in $PM_{2.5}$ levels in Houston are associated with a highly recirculating sea breeze. Environ. Pollut. 366, 125381. https://doi.org/10.1016/j.envpol.2024.125381.

Chen, D., Wang, X., Nelson, P., Li, Y., Zhao, N., Zhao, Y., Lang, J., Zhou, Y., Guo, X., 2017. Ship emission inventory and its impact on the $PM_{2.5}$ air pollution in Qingdao Port, North China. Atmos. Environ. 166, 351–361. https://doi.org/10.1016/j.atmosenv.2017.07.021.

Chen, Z., Xie, X., Cai, J., Chen, D., Gao, B., He, B., Cheng, N., Xu, B., 2018. Understanding meteorological influences on $PM_{2.5}$ concentrations across China: a temporal and spatial perspective. Atmos. Chem. Phys. 18, 5343–5358. https://doi.org/10.5194/acp-185343-2018.

Choi, D., Ham, J., Heo, G., Lee, S.H., Yoo, J.W., Yang, G.H., Jeon, S., Kim, C.H., 2024. Mesoscale wind field patterns conducive to the high-$PM_{2.5}$ episodes over South Korea: cluster analysis. Atmos. Environ. 333, 120653. https://doi.org/10.1016/j.atmosenv.2024.120653.

Crippa, M., Guizzardi, D., Muntean, M., Schaaf, E., Monforti-Ferrario, F., Banja, M., Pagani, F., Solazzo, E., 2022. EDGAR v6.1 global air pollutant emissions. Eur. Comm. Joint Res. Cent. (JRC129555). https://edgar.jrc.ec.europa.eu/dataset_ap61.

Crosman, E.T., Horel, J.D., 2010. Sea and Lake Breezes: A Review of Numerical Studies. Boundary-Layer Meteorol 137, 1–29. https://doi.org/10.1007/s10546-010-9517-9.

Ding, J., Dai, Q., Zhang, Y., Xu, J., Huangfu, Y., Feng, Y., 2021. Air humidity affects secondary aerosol formation in different pathways. Sci. Total Environ. 759, 143540. https://doi.org/10.1016/j.scitotenv.2020.143540.

Emery, C., Tai, E., Yarwood, G., 2001. Enhanced meteorological modeling and performance evaluation for two Texas ozone episodes. Env. Int. Corp. 161, 235.

Gipson, G.L., Young, J., 1999. Process Analysis. in Science Algorithms of the EPA models-3 Community Multiscale Air Quality (CMAQ) Modeling System, Chap. 16, EPA/600/R-99/030. https://www.cmascenter.org/cmaq/science_documentation/pdf/ch16.pdf. (Accessed 4 July 2020).

Han, Z., Wang, Y., Xu, J., Shang, Y., Li, Z., Lu, C., Zhan, P., Song, X., Lv, M., Yang, Y., 2024. Assessment of multiple planetary boundary layer height retrieval methods and their impact on $PM_{2.5}$ and its chemical compositions throughout a year in Nanjing. Remote Sens. 16 (18), 3464. https://doi.org/10.3390/rs16183464.

He, J., Chen, D., Gu, Y., Jia, H., Zhong, K., Kang, Y., 2022. Evaluation of planetary boundary layer schemes in WRF model for simulating sea-land breeze in Shanghai, China. Atmos. Res. 278, 106337. https://doi.org/10.1016/j.atmosres.2022.106337.

Hong, S.Y., Noh, Y., Dudhia, J., 2006. A new vertical diffusion package with an explicit treatment of entrainment processes. Mon. Weather Rev. 134 (9), 2318–2341. https://doi.org/10.1175/MWR3199.1.

Huang, Q., Cai, X., Wang, J., Song, Y., Zhu, T., 2018. Climatological study of the Boundary-layer air Stagnation Index for China and its relationship with air pollution. Atmos. Chem. Phys. 18 (10), 7573–7593. https://doi.org/10.5194/acp-18-7573-2018.

Huang, Y., Li, S., Zhu, Y., Liu, Y., Hong, Y., Chen, X., Deng, W., Xi, X., Lu, X., Fan, Q., 2025. Increasing sea-land breeze frequencies over coastal areas of China in the past five decades. Geophys. Res. Lett. 52 (4). https://doi.org/10.1029/2024GL112480 e2024GL112480.

Iacono, M.J., Delamere, J.S., Mlawer, E.J., Shephard, M.W., Clough, S.A., Collins, W.D., 2008. Radiative forcing by long-lived greenhouse gases: calculations with the AER radiative transfer models. J. Geophys. Res. Atmos. 113, 2–9. https://doi.org/10.1029/2008JD009944.

Jacob, D.J., Winner, D.A., 2009. Effect of climate change on air quality. Atmos. Environ. 43 (1), 51–63. https://doi.org/10.1016/j.atmosenv.2008.09.051.

Jang, E., Choi, S., Yoo, E., Hyun, S., An, J., 2023. Impact of shipping emissions regulation on urban aerosol composition changes revealed by receptor and numerical modelling. npj Clim. Atmos. Sci. 6, 1–13. https://doi.org/10.1038/s41612-023-00364-9.

Jeong, Y.C., Yeh, S.W., Jeong, J.I., Park, R.J., Yoo, C., Yoon, J.H., 2023. Intrinsic atmospheric circulation patterns associated with high $PM_{2.5}$ concentration days in South Korea during the cold season. Sci. Total Environ. 863, 160878. https://doi.org/10.1016/j.scitotenv.2022.160878.

Kwon, J.W., Yeo, S., Lee, W.J., 2023. Assessment of shipping emissions on Busan port of South Korea. J. Mar. Sci. Eng. 11 (4). https://doi.org/10.3390/jmse11040716.

Lee, S., Kim, J.H., Kim, M.K., Lee, S.H., Kim, C.H., 2025. Synergistic effects of synoptic and quasi-biweekly timescale atmospheric circulation patterns on $PM_{2.5}$ concentration in South Korea. Atmos. Environ. 348, 121122. https://doi.org/10.1016/j.atmosenv.2025.121122.

Lee, S.H., Park, G.Y., Chang, L.S., Song, C.K., 2015. Behavior of air particles associated with atmospheric recirculation over complex coastal area. Asia-Pacific J. Atmos. Sci. 51, 311–322. https://doi.org/10.1007/s13143-015-0080-7.

Li, H., Wang, B., Fang, X., Zhu, W., Fan, Q., Liao, Z., Liu, J., Zhang, A., Fan, S., 2018. Combined effect of boundary layer recirculation factor and stable energy on local air quality in the Pearl River Delta over southern China. J. Air Waste Manag. Assoc. 68 (7), 685–699. https://doi.org/10.1080/10962247.2018.1439125.

Li, W., Wang, Y., Bernier, C., Estes, M., 2020. Identification of sea breeze recirculation and its effects on ozone in Houston, TX, during DISCOVER-AQ 2013. J. Geophys. Res. Atmos. 125 (22). https://doi.org/10.1029/2020JD033165 e2020JD033165.

Lin, Y., Wang, Y., Pan, B., Hu, J., Guo, S., Levy Zamora, M., Tian, P., Su, Q., Ji, Y., Zhao, J., Gomez-Hernandez, M., Hu, M., Zhang, R., 2022. Formation, radiative forcing, and climatic effects of severe regional haze. Atmos. Chem. Phys. 22 (7), 4951–4967. https://doi.org/10.5194/acp-22-4951-2022.

Lu, D., Li, H., Tian, M., Wang, G., Qin, X., Zhao, N., Huo, J., Yang, F., Lin, Y., Chen, J., Fu, Q., Duan, Y., Dong, X., Deng, C., Abdullaev, S.F., Huang, K., 2023. Secondary aerosol formation during a special dust transport event: impacts from unusually enhanced ozone and dust backflows over the ocean. Atmos. Chem. Phys. 23, 13853–13868. https://doi.org/10.5194/acp-23-13853-2023.

Lv, Z., Liu, H., Ying, Q., Fu, M., Meng, Z., Wang, Y., Wei, W., Gong, H., He, K., 2018. Impacts of shipping emissions on $PM_{2.5}$ pollution in China. Atmos. Chem. Phys. 18 (21), 15811–15824. https://doi.org/10.5194/acp-18-15811-2018.

Meng, L., Yang, E., Liu, L., Wang, W., Yang, J., Qu, P., 2024. Impacts of sea land breeze on the Fog and $PM_{2.5}$ concentration in Tianjin, China. Aerosol Air Qual. Res. 24 (8). https://doi.org/10.4209/aaqr.230279.

Miao, Y., Guo, J., Liu, S., Liu, H., Li, Z., Zhang, W., Zhai, P., 2017. Classification of summertime synoptic patterns in Beijing and their associations with boundary layer structure affecting aerosol pollution. Atmos. Chem. Phys. 17, 3097–3110. https://doi.org/10.5194/acp-17-3097-2017.

Miller, S.T.K., Keim, B.D., Talbot, R.W., Mao, H., 2003. Sea breeze: structure, forecasting, and impacts. Rev. Geophys. 41. https://doi.org/10.1029/2003RG000124.

Morrison, H., Thompson, G., Tatarskii, V., 2009. Impact of cloud microphysics on the development of trailing stratiform precipitation in a simulated squall line: comparison of one- and two-moment schemes. Mon. Weather Rev. 137 (3), 991–1007. https://doi.org/10.1175/2008MWR2556.1.

Oh, H.R., Park, D.S.R., Kim, D., Ho, C.H., Lee, S., 2024. Synoptic circulation factors associated with wintertime high-$PM_{2.5}$ concentrations in seoul, Republic of Korea: their interpretations and applications. Atmos. Environ. 325, 120444. https://doi.org/10.1016/j.atmosenv.2024.120444.

Oh, I.B., Kim, Y.K., Lee, H.W., Kim, C.H., 2006. An observational and numerical study of the effects of the late sea breeze on ozone distributions in the Busan metropolitan area, Korea. Atmos. Environ. 40, 1284–1298. https://doi.org/10.1016/j.atmosenv.2005.10.049.

Park, S.Y., Lee, S.H., Lee, H.W., 2014. Assimilation of wind profiler observations and its impact on three-dimensional transport of ozone over the Southeast Korean Peninsula. Atmos. Environ. 99, 660–672. https://doi.org/10.1016/j.atmosenv.2014.09.082.

Qu, K., Yan, Y., Wang, X., Jin, X., Vrekoussis, M., Kanakidou, M., Brasseur, G.P., Lin, T., Xiao, T., Cai, X., Zeng, L., Zhang, Y., 2024. The effect of cross-regional transport on ozone and particulate matter pollution in China: a review of methodology and current knowledge. Sci. Total Environ. 947, 174196. https://doi.org/10.1016/j.scitotenv.2024.174196.

Russo, A., Gouveia, C.M., Soares, P.M.M., Cardoso, R.M., Mendes, M.T., Trigo, R.M., 2018. The unprecedented 2014 Legionnaires' disease outbreak in Portugal: atmospheric driving mechanisms. Int. J. Biometeorol. 62, 1167–1179. https://doi.org/10.1007/s00484-018-1520-8.

Russo, A., Gouveia, C., Levy, I., Dayan, U., Jerez, S., Mendes, M., Trigo, R., 2016. Coastal recirculation potential affecting air pollutants in Portugal: the role of circulation weather types. Atmos. Environ. 135, 9–19. https://doi.org/10.1016/j.atmosenv.2016.03.039.

Sarwar, G., Luecken, D., Yarwood, G., Whitten, G.Z., Carter, W.P.L., 2008. Impact of an updated carbon bond mechanism on predictions from the CMAQ modeling system: preliminary assessment. J. Appl. Meteorol. Climatol. 47 (1), 3–14. https://doi.org/10.1175/2007JAMC1393.1.

Shao, M., Xu, X., Lu, Y., Dai, Q., 2023. Spatio-temporally differentiated impacts of temperature inversion on surface $PM_{2.5}$ in eastern China. Sci. Total Environ. 855, 158785. https://doi.org/10.1016/j.scitotenv.2022.158785.

Skamarock, W.C., Klemp, J.B., Dudhia, J., Gill, D.O., Barker, D.M., Duda, M.G., Huang, X.-Y., Wang, W., Powers, J.G., 2008. A description of the advanced research WRF version 3. NCAR Tech. Note NCAR/TN-468+STR 113.

Viner, B., Noble, S., Qian, J.H., Werth, D., Gayes, P., Pietrafesa, L., Bao, S., 2021. Frequency and characteristics of inland advecting sea breezes in the Southeast United States. Atmosphere 12 (8). https://doi.org/10.3390/atmos12080950.

Wang, T., Du, H., Zhao, Z., Russo, A., Zhang, J., Zhou, C., 2022. The impact of potential recirculation on the air quality of Bohai Bay in China. Atmos. Pollut. Res. 13 (1), 101268. https://doi.org/10.1016/j.apr.2021.101268.

Whitten, G.Z., Heo, G., Kimura, Y., McDonald-Buller, E., Allen, D.T., Carter, W.P.L., Yarwood, G., 2010. A new condensed toluene mechanism for carbon bond: CB05-TU. Atmos. Environ. 44 (40), 5346–5355. https://doi.org/10.1016/j.atmosenv.2009.12.029.

Yoo, J.W., Lee, S.H., 2025. Characteristics of local recirculation affecting summer ozone in coastal areas of the Korean Peninsula. Atmos. Res. 315, 107934. https://doi.org/10.1016/j.atmosres.2025.107934.

Yoo, J.W., Park, S.Y., Jeon, W., Jung, J., Park, J., Mun, J., Kim, D., Lee, S.H., 2024a. Understanding the physical mechanisms of $PM_{2.5}$ formation in Seoul, Korea: assessing the role of aerosol direct effects using the WRF-CMAQ model. Air Qual. Atmos. Health 17 (8), 1701–1714. https://doi.org/10.1007/s11869-024-01538-x.

Yoo, J.W., Park, S.Y., Jo, H.Y., Jeong, Y., Lee, H.J., Kim, Cheol-Hee, Lee, S.H., 2024b. Assessing the role of cold front passage and synoptic patterns on air pollution in the Korean Peninsula. Environ. Pollut. 348, 123803. https://doi.org/10.1016/j.envpol.2024.123803.

Yoo, J.W., Park, S.Y., Lee, K., Lee, D., Lee, Y., Lee, S.H., 2022. Impacts of plateau-induced lee troughs on regional $PM_{2.5}$ over the Korean Peninsula. Atmos. Pollut. Res. 13 (7), 101459.

Yu, C., Zhao, T., Bai, Y., Zhang, L., Yu, X., Kong, S., He, J., Cui, C., Yang, J., You, Y., Ma, G., Wu, M., Chang, J., 2020. Heavy air pollution with a unique "non-stagnant" atmospheric boundary layer in the Yangtze River middle basin aggravated by regional transport of $PM_{2.5}$ over China. Atmos. Chem. Phys. 20 (12), 7217–7230.

Zhong, J., Zhang, X., Wang, Y., Sun, J., Zhang, Y., Wang, J., Tan, K., Shen, X., Che, H., Zhang, L., Zhang, Z., Qi, X., Zhao, H., Ren, S., Li, Y., 2017. Relative contributions of boundary-layer meteorological factors to the explosive growth of $PM_{2.5}$ during the red-alert heavy pollution episodes in Beijing in December 2016. J. Meteorol. Res. 31, 809–819. https://doi.org/10.1007/s13351-017-7088-0.